Inorganic Chemistry

Article

pubs.acs.org/IC

Electrochemical and Spectroscopic Investigation of Ln^{3+} (Ln = Sm, Eu, and Yb) Solvation in Bis(trifluoromethylsulfonyl)imide-Based Ionic Liquids and Coordination by *N,N,N′,N′*-Tetraoctyl-3-oxa-pentane Diamide (TODGA) and Chloride

Yunfeng Pan and Charles L. Hussey*

Department of Chemistry and Biochemistry, The University of Mississippi, University, Mississippi 38677, United States

ABSTRACT: The electrochemistry and electronic absorption spectroscopy of samarium, europium, and ytterbium were investigated in the 1-(1-butyl)-trimethylammonium bis(trifluoromethylsulfonyl)imide ($BuMe_3NTf_2N$) and 1-butyl-3-methylpyrrolidinium bis(trifluoromethylsulfonyl)imide ($BuMePyroTf_2N$) ionic liquids and in these solvents containing the neutral tridentate ligand *N,N,N′,N′*-tetraoctyl-3-oxo-pentane diamide (TODGA) and the anionic hard ligand chloride. Lanthanide ions were introduced into the ionic liquids by controlled potential oxidation of the respective metals to yield solutions containing Eu^{2+}, Sm^{3+}, and Yb^{3+}, and it was possible to cycle between Eu^{2+} and Eu^{3+} as well as Yb^{3+} and Yb^{2+} using controlled potential electrolysis. Electronic absorption spectroscopy suggested that the Ln^{3+} species are weakly solvated by Tf_2N^- anions as $[Ln(Tf_2N)_x]^{(x-3)-}$ in the neat ILs. The quasireversible $Ln^{3+/2+}$ couples of all three elements were readily accessible in these ILs, but Sm^{2+} was only stable on the voltammetric time scale. Addition of TODGA to $[Ln(Tf_2N)_x]^{(x-3)-}$ solutions produces 3:1 complexes with Eu^{3+} and Sm^{3+} but only a 2:1 complex with the smaller Yb^{3+} ion. Depending on the temperature, addition of Cl^- to solutions of $[Ln(Tf_2N)_x]^{(x-3)-}$ induces precipitation of $LnCl_3(s)$ when the mole ratio $mCl^-/mLn^{3+} \approx 3$. However, when $mCl^-/mLn^{3+} > 3$, these precipitates redissolve to form the octahedral chloride complexes, $[LnCl_6]^{3-}$.

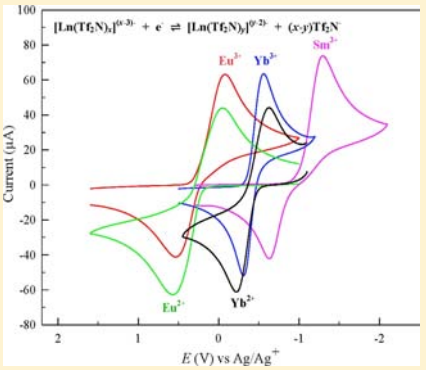

INTRODUCTION

Anhydrous, hydrophobic room-temperature ionic liquids (ILs) based on bis(trifluoromethylsulfonyl)imide (Tf_2N^-) anions are versatile solvents for chemistry and electrochemistry.[1−4] Among the many different classes of ILs that have been prepared and studied to date, Tf_2N-based systems typically exhibit lower viscosities, higher ionicities and electrical conductivities, and extended anodic potential windows. As a general rule, these systems are more chemically and thermally robust than ILs prepared with anions such as BF_4^- or PF_6^-. Furthermore, when prepared from quaternary ammonium cations that are based on alkyl rather than aromatic substituents, Tf_2N-based ILs also have very favorable cathodic potential windows. Some examples include 1-(1-butyl)-1-methylpyrrolidinium bis(trifluoromethylsulfonyl)imide ($BuMePyroTf_2N$) and 1-(1-butyl)trimethylammonium bis(trifluoromethylsulfonyl)imide ($BuMe_3NTf_2N$).

There is developing interest in using ILs as substitutes for the volatile organic solvents currently employed in the reprocessing of spent nuclear fuel (SNF)[5,6] and as solvents for actinide (An) and lanthanide (Ln) chemistry in general.[7,8] However, relatively little is known about the solvation of actinide and lanthanide ions in these ILs, particularly those based on Tf_2N^-. In addition, these ILs provide a novel ionic matrix for investigating the coordination of dissolved An and Ln ions with simple ligands such as chloride and with more elaborate neutral polydentate ligands such as *N,N,N′,N′*-tetraoctyl-3-oxa-pentane diamide (TODGA). TODGA is proposed as a liquid−liquid extraction agent for recovering trivalent An and Ln ions from SNF with hydrophobic ILs.[9−14]

It is well established that samarium, europium, and ytterbium are relatively unique among the lanthanide elements because of their proclivity to form stable, discrete Ln^{2+} species. For Eu^{2+} and Yb^{2+}, this is explained in part by the stability afforded by the $4f^7$ and $4f^{14}$ electronic configurations of these ions. The Ln^{3+} ions of these elements are often employed as surrogates for the minor actinides found in SNF, which are commonly found as trivalent species. Samarium, europium, and ytterbium also present an interesting contrast in terms of their trivalent ionic radii and $Ln^{3+/2+}$ reduction potentials (versus NHE) in aqueous solution: Sm^{3+} (95.8 pm, −1.55 V), Eu^{3+} (94.7 pm, −0.35 V), and Yb^{3+} (86.8 pm, −1.05 V).[15,16]

The absorption spectra of Ln^{3+} species are very interesting in their own right. Typically, they consist of groups of narrow bands, similar in appearance to atomic spectra, because the 4f valence shell is shielded from the environment around the lanthanide ion by higher lying closed shells.[17,18] These bands are due to the intraconfigurational 4f ← 4f transitions, which are much narrower than the broad bands found in d-group

Received: December 14, 2012
Published: February 25, 2013

   dx.doi.org/10.1021/ic3027557 | *Inorg. Chem.* 2013, 52, 3241−3252

absorption spectra. Also, the intensities of 4f ← 4f transitions are usually very weak, because this type of transition is forbidden by the Laporte selection rule. The spectroscopic behavior of Ln^{2+} ions differs greatly from that of Ln^{3+} ions. Here the electronic spectra consist of intense broad bands due to 5d ← 4f transitions. Overall, with the exception of Ce^{3+}, Er^{3+}, Eu^{2+}, Eu^{3+}, and Nd^{3+},[19−25] there is a relative lack of information about the electronic absorption spectra of lanthanide ions in Tf_2N-based ILs.

The electrochemical behavior of the $Ln^{3+/2+}$ (Ln = Sm, Eu, and Yb) couples has been examined in Tf_2N-based and closely related ILs. For example, Bhatt et al.[26,27] described the preparation and electrochemistry of the hydrate complexes, $[Ln(Tf_2N)_3(H_2O)_3]$ (Ln = La^{3+}, Sm^{3+}, Eu^{3+}), in $BuMe_3NTf_2N$ and similar ILs. In addition to observing the quasireversible $Sm^{3+/2+}$ and $Eu^{3+/2+}$ couples, they obtained evidence suggesting that all three trivalent species can be electrochemically reduced to Ln^0, but the deposits were not stable and gave no appreciable stripping currents. Yamagata et al.[28] conducted a detailed investigation of the electrochemistry of Sm, Eu, and Yb in 1-ethyl-3-methylimidazolium bis(trifluoromethylsulfonyl)imide ($EtMeImTf_2N$) and $BuMePyroTf_2N$. They reported that the $Sm^{3+/2+}$, $Eu^{3+/2+}$, and $Yb^{3+/2+}$ reactions were quasireversible and presented diffusion coefficients for each trivalent species. Luminescence spectroscopy and voltammetry were used to examine the coordination of Eu^{3+} in Tf_2N-based ionic liquids before and after the addition of H_2O.[29] The $Eu^{3+/2+}$ reaction was found to be quasireversible in the ILs but reported to be nearly reversible in aqueous solution. Rao et al.[30] examined the electrochemistry of Eu^{3+} in $BuMePyroTf_2N$. In addition to measuring the heterogeneous electron-transfer rate constant for the $Eu^{3+/2+}$ reaction and the diffusion coefficient for Eu^{3+}, they reported that Eu^{2+} could be reduced to Eu^0 at glassy carbon, which they confirmed with energy-dispersive X-ray spectroscopy. However, there was no appreciable stripping current for the deposit. Cyclic voltammetry was used to investigate the ion exchange between the trifluoromethanesulfonate anion (OTf^-) and the less basic Tf_2N^- anion coordinated with Yb^{3+} in the corresponding BuMePyro-based ILs.[31]

In this investigation, we used electronic absorption spectroscopy to probe the coordination of Sm^{3+}, Eu^{3+}, Eu^{2+}, Yb^{3+}, and Yb^{2+} in the Tf_2N-based ILs, $BuMePyroTf_2N$ and $BuMe_3NTf_2N$. (The physical and chemical properties of these two ILs are very similar,[32] and they were used interchangeably during this investigation as indicated.) The spectral data for Sm^{3+}, Yb^{3+}, and Yb^{2+} appear to be the first reported for these lanthanide ions in Tf_2N-based ILs. The diffusion coefficients of these ions were measured by using rotating disk electrode voltammetry, whereas electrochemical impedance spectroscopy was used to estimate the formal heterogeneous electron-transfer rate constants of the $Eu^{3+/2+}$ and $Yb^{3+/2+}$ reactions. Finally, amperometric titration experiments based on cyclic staircase voltammetry were used to probe the stoichiometry of the complexes formed between Sm^{3+}, Eu^{3+}, and Yb^{3+} and both TODGA and Cl^-.

EXPERIMENTAL SECTION

Ionic Liquids and Lanthanide Metals. The sources and purities of $BuMe_3NTf_2N$, $BuMePyroTf_2N$, and BuMePyroCl used in this investigation, including the water content, as well as any necessary purification procedures, have been described in a previous paper.[32] Samarium, europium, and ytterbium metals (Alfa AESAR, 99.98%) were used as purchased. Because of the established reactivity of these lanthanide metals with moisture and oxygen, all experiments were performed inside a glovebox with a nitrogen-filled atmosphere. The glovebox atmosphere quality was tested with a 25 W light bulb whose filament was exposed to the glovebox atmosphere.[33]

Electrochemical Instrumentation and Experiments. Cyclic staircase voltammetry (CSV), rotating disk electrode voltammetry (RDEV), and controlled potential electrolysis (CPE) experiments were performed with an EG&G Princeton Applied Research (PAR) model 263A potentiostat/galvanostat. Electrochemical data were recorded on a desktop computer using PAR model 270 Electrochemical Analysis Software. Electronic resistance compensation was employed during all potential sweep experiments. For electrochemical impedance spectroscopy (EIS) measurements, a PAR frequency response detector (FRD 100) was mated to the PAR model 263A potentiostat/galvanostat. With the electrochemical cell described below, this system provided useful impedance measurements over the linear frequency range from 100 kHz to 100 mHz. The resulting EIS data were analyzed with ZsimpWin Electrochemical Impedance Spectroscopy Analysis Software (PAR Rev. 3.22).

The cells and Pt-RDE working electrodes used for CSV and RDEV were the same as those described previously.[32] CPE experiments were carried out by employing large surface area Pt or lanthanide metal coupons as the working electrodes. A BASi MF-2062 nonaqueous Ag^+/Ag reference electrode, which contained 0.01 M $AgNO_3$ and 0.1 M Bu_4NPF_6 dissolved in CH_3CN, served as the reference electrode for all experiments. $E_{1/2}$ of the Fc^+/Fc couple in the ILs was 0.072 V versus this reference electrode. The counter electrode consisted of a platinum wire spiral immersed in the corresponding IL, but separated from the bulk IL by a porosity E glass frit (ACE Glass). EIS experiments were performed outside the glovebox using the same cell described previously.[34] The working electrode for these experiments was a miniature BASi glassy carbon disk electrode (geometrical area = 0.0707 cm^2). All working electrodes were carefully polished with 1.0, 0.3, and 0.05 μm alumina (Buehler) on a Buehler Metaserv grinder-polisher before their initial use or after long periods of storage.

Electronic Absorption Spectroscopy. Electronic absorption spectra were acquired outside the glovebox in 1 or 10 mm path length fused silica cells fitted with airtight Teflon caps. All spectra were recorded at room temperature with a Shimadzu UV-1600 UV−visible spectrophotometer.

RESULTS AND DISCUSSION

Electrochemical Preparation of Ionic Liquid Solutions Containing $Ln^{3+}$and Ln^{2+}. Solutions of Sm^{3+}, Eu^{2+}, and Yb^{3+} were prepared by CPE oxidation of the respective metals at an applied potential of 0.6 V. The oxidation states, n, of the dissolved lanthanide species were calculated from the change in the weight, Δw, of the Ln metals after passage of a given charge, Q_{exp}, using Faraday's law

Table 1. Anodic Dissolution of Lanthanide Metals

lanthanide metal	Δw (g)	Q_{exp} (C)	n	n_{avg}
Sm	0.0108	20.5	2.96	3.0 ± 0.1[a]
	0.0105	18.9	2.80	
	0.0098	19.5	3.10	
Eu	0.0316	38.9	1.94	2.0 ± 0.0[a]
	0.0246	31.4	2.01	
	0.0240	30.0	1.97	
Yb	0.0190	31.6	2.98	2.9 ± 0.1[a]
	0.0395	63.6	2.89	
	0.0191	30.0	2.82	

[a]Average deviation from the mean

dx.doi.org/10.1021/ic3027557 | Inorg. Chem. 2013, 52, 3241−3252

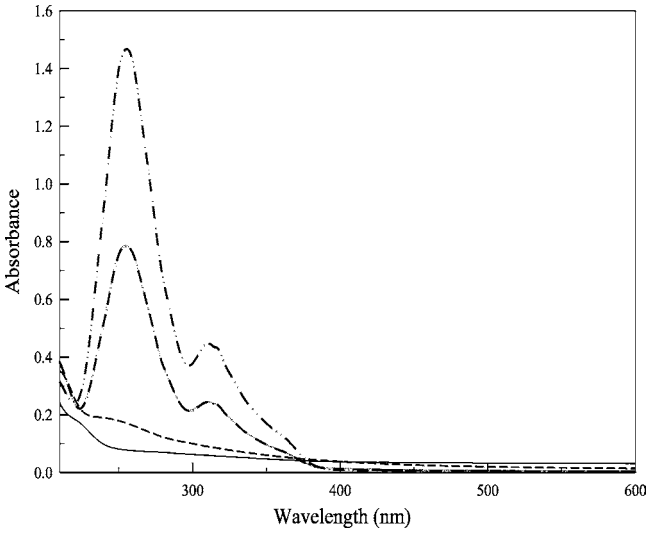

Figure 1. Electronic absorption spectra of Eu^{2+} and Eu^{3+} in $BuMe_3NTf_2N$: (—) neat ionic liquid versus air; (– –) 5 mM Eu^{3+}; (– · –) 2.5 mM Eu^{2+} + 2.5 mM Eu^{3+}; (– · · –) 5 mM Eu^{2+}.

$$n = MQ_{exp}/F\Delta w \quad (1)$$

where M is the atomic mass of the Ln metal and F is the Faraday constant. The charge passed during these experiments was determined with the coulometer feature of the potentiostat. The results of these experiments are given in Table 1, and they verify that the species introduced using this method are indeed Sm^{3+}, Eu^{2+}, and Yb^{3+}. Solutions containing Eu^{3+} and Yb^{2+} were also generated by CPE. The former was prepared by exhaustive oxidation of Eu^{2+} solutions at a potential of 1.2 V. Likewise, solutions of Yb^{2+} were obtained by CPE reduction of dissolved Yb^{3+} at a potential of −1.2 V. Using a large area Pt-gauze working electrode, it was possible to cycle efficiently between Eu^{2+} and Eu^{3+} as well as between Yb^{3+} and Yb^{2+} with CPE. Attempts to electrochemically generate solutions containing Sm^{2+} were not successful because this divalent species is not stable in the IL on the time scale of CPE. Similar results have been noted for divalent Ce^{2+} [25] as well as divalent Pr^{2+} and Nd^{2+} [35] in this ionic liquid. The instability of divalent samarium is somewhat surprising because the halide salts are well established, and compounds such as SmI_2 are commercially available.

This electrolytic method for preparing solutions of lanthanide ions is advantageous because it is not based on dissolution of compounds or complexes with anions different from Tf_2N^- and/or compounds that contain water of hydration. Therefore, the resulting soluble Ln^{x+} (x = 2 or 3) species can only be solvated or coordinated by Tf_2N^- anions. Electronic absorption spectroscopy was used to investigate the coordination of these species in the IL and is reported below. However, one complication noticed when introducing lanthanide ions with this electrochemical method is that during the course of electrolysis the surface of the Ln^0 electrodes becomes covered with a black film. Data in Table 1 indicate that this film contributes virtually nothing to the mass change used with eq 1 to determine n, and the film did not lead to passivation of the electrode surface. Although we did not attempt to analyze this film, we speculate that it results from localized reduction of the IL at the freshly exposed Ln^0 surface. We believe that this film is similar to the solid electrolyte interface (SEI) layer found when active metals such as Li^0 are

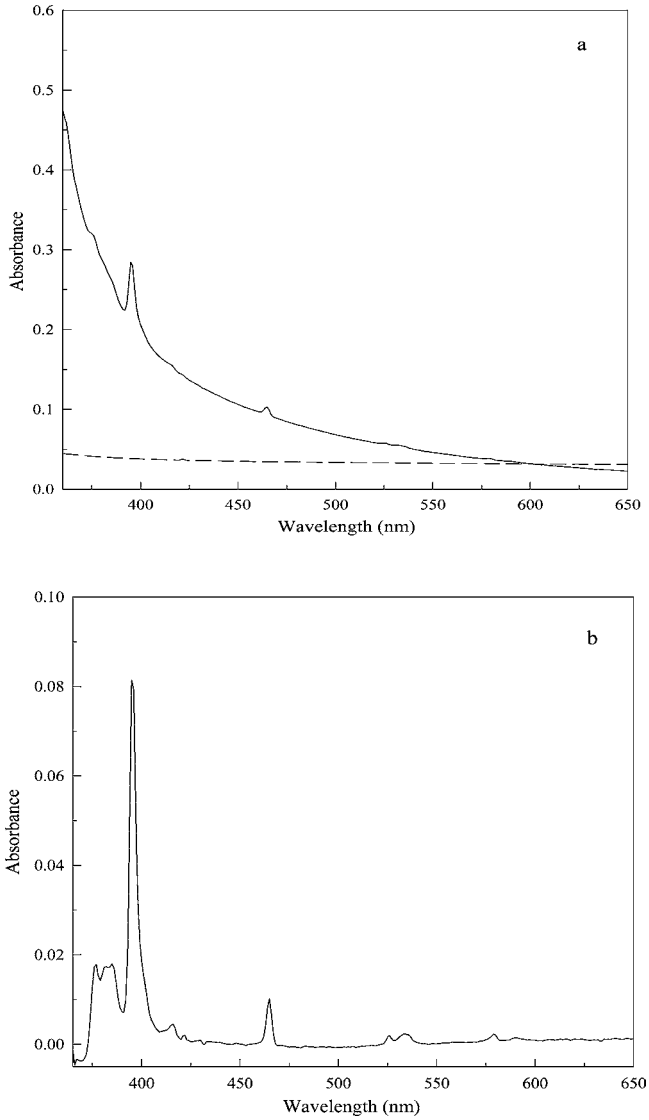

Figure 2. Electronic absorption spectra of 40 mM Eu^{3+} in $BuMe_3NTf_2N$: (a) before and (b) after background correction. Dashed line: pure ionic liquid.

anodized in ILs.[36] A similar phenomenon was observed during the oxidation of Ce^0 to Ce^{3+}.[25] These results suggest that the lanthanide metals, like Li^0, are sufficiently active to reduce the ILs solvents used in this investigation. Interestingly, no obvious film formation is observed on the Ln coupons used for these experiments, i.e., if they are immersed in the IL for several days before anodization; they appear to be perfectly stable. In fact, they must be polished with emery paper before an appreciable dissolution current can be achieved. We conclude that when first received from the supplier in sealed containers, they are covered by a very thin adventitious oxide film.

Electronic Absorption Spectroscopy of Lanthanide Ions. Absorption spectra of Eu^{2+} are given in Figure 1, and they show the spectral changes resulting from oxidation of Eu^{2+} to Eu^{3+} in $BuMe_3NTf_2N$. The spectrum of Eu^{2+} exhibits two moderately intense absorption bands at 256 and 313 nm. These broad bands are due essentially to $4f^65d \leftarrow 4f^7$ transitions,[37] where the excited configuration is split by the ligand field of Tf_2N^- into several levels given by $J_1\Gamma_n$.[38] The molar absorptivities for these bands were estimated to be 2380 and

dx.doi.org/10.1021/ic3027557 | Inorg. Chem. 2013, 52, 3241−3252

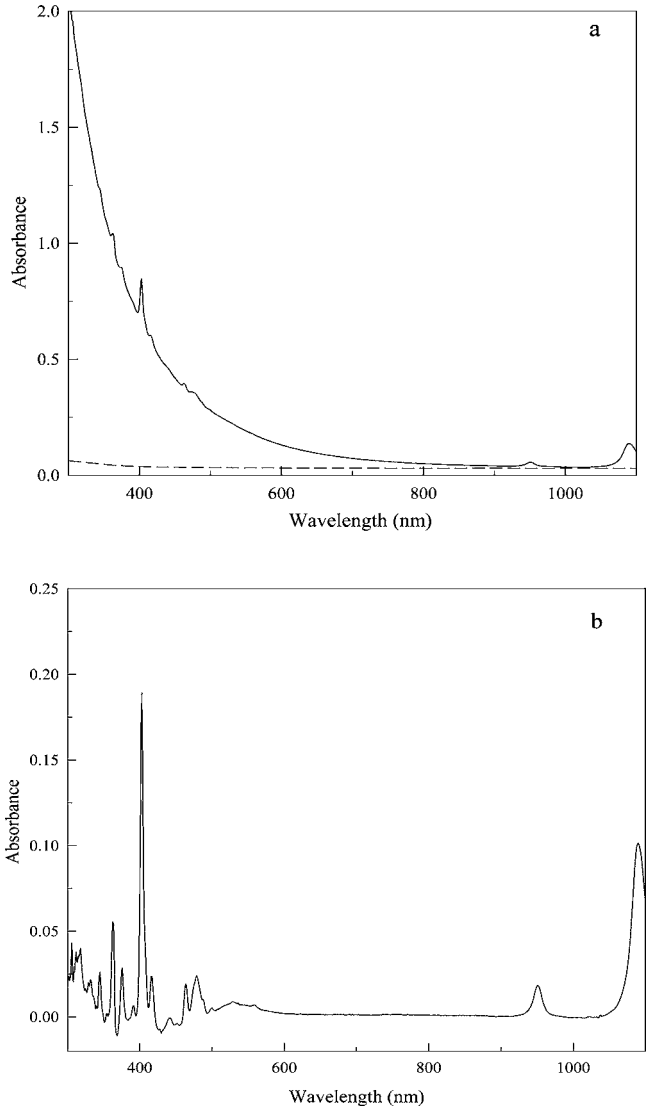

Figure 3. Electronic absorption spectra of 50 mM Sm^{3+} in $BuMe_3NTf_2N$: (a) before and (b) after background correction. Dashed line: pure ionic liquid.

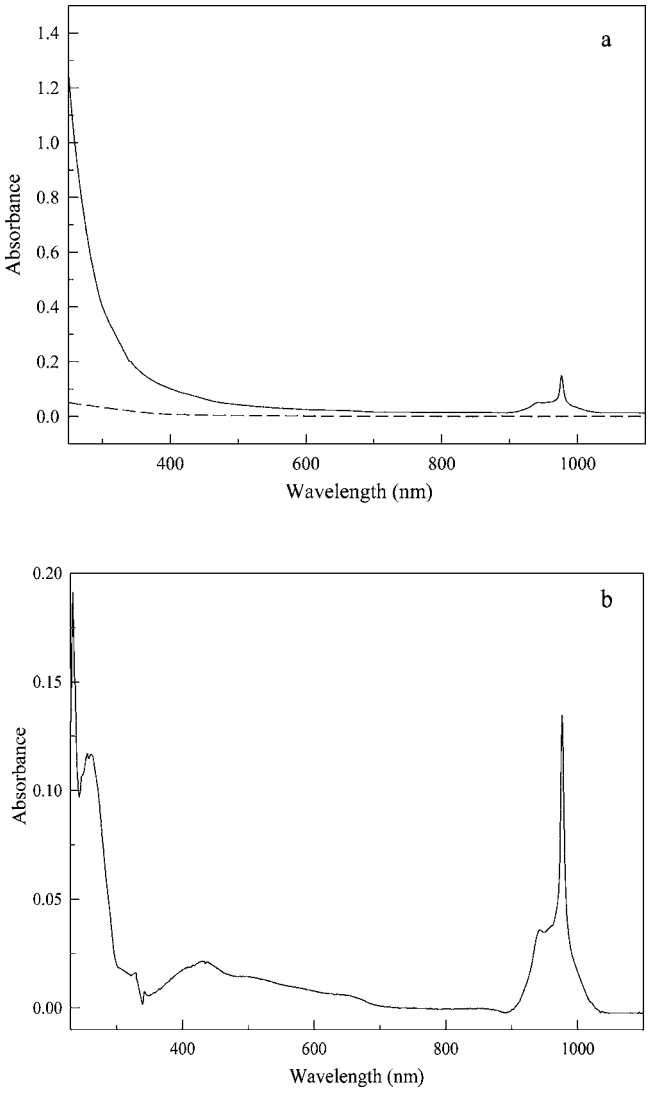

Figure 4. Electronic absorption spectra of 30 mM Yb^{3+} in $BuMePyroTf_2N$: (a) before and (b) after background correction. Dashed line: pure ionic liquid.

300 L mol^{-1} cm^{-1}, respectively. The spectrum of Eu^{2+} in $BuMe_3NTf_2N$ is very similar to that reported for weakly solvated Eu^{2+} in acetonitrile and aqueous solutions[37,39] and also very similar to $EuCl_2$ dissolved in water and methanol.[40−42] However, the spectrum of Eu^{2+} in the related $BuMeImPF_6$ ionic liquid is somewhat different in that these bands are shifted to 290 and 355 nm, respectively, implying that the solvation environment provided by PF_6^- is somewhat different from that associated with Tf_2N^-.[19] Figure 1 also shows the spectrum obtained after 50% of the Eu^{2+} was oxidized to Eu^{3+}; the absorbances of the Eu^{2+} bands decreased commensurately. After all of the Eu^{2+} is oxidized to Eu^{3+}, the two Eu^{2+} absorption bands have completely disappeared. No new absorption bands could be observed because the intraconfigurational 4f ← 4f transitions associated with Eu^{3+} are too weak to be observed at a solution concentration of 5 mM.

In order to observe the very weak absorption bands expected for IL solutions of the three trivalent lanthanide ions it was necessary to prepare very concentrated solutions. Unfortunately, it was found that the spectra of these solutions routinely displayed a baseline that increased exponentially with decreasing wavelength as shown for Eu^{3+} in Figure 2a. Such behavior is typical of Rayleigh scattering, which is due to elastic scattering by particles with diameters smaller than the wavelength of light. Particles may be individual atoms or molecules, but in this case, they may be particles of impurities such as silica entrapped in the lanthanide metals that are released during oxidation. Note that this scattering phenomenon is absent in the neat IL. Thus, we developed a simple method to subtract the baseline from spectra distorted by scattering so that the spectral bands could be resolved. This method is adapted from that used by Agilent Technologies UV−visible ChemStation software to correct for scattering in pharmaceutical samples. In order to apply this method, we first removed all obvious absorption bands from the raw experimental data set to leave only the baseline data. Second, an exponential decay equation, eq 2, was fitted to this baseline data using SigmaPlot software.

$$f = y^0 + ae^{-bx} + ce^{-dx} \quad (2)$$

The constants resulting from this fit were used to generate an artificial baseline that was subtracted from the complete

dx.doi.org/10.1021/ic3027557 | Inorg. Chem. 2013, 52, 3241−3252

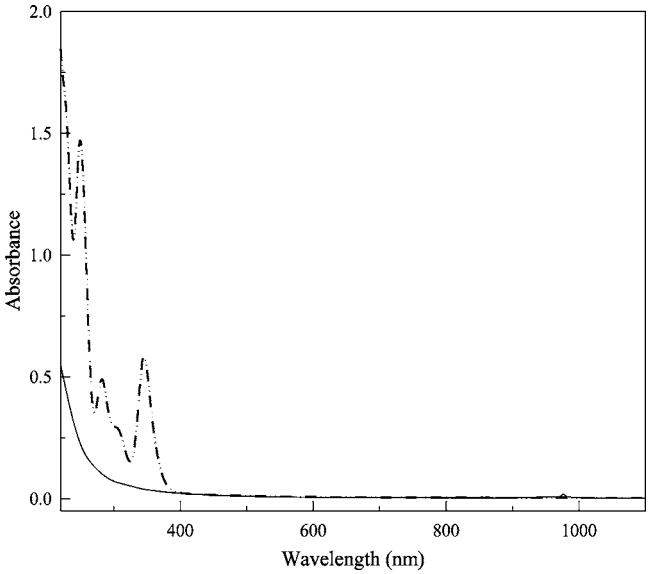

Figure 5. Electronic absorption spectra of Yb^{2+} and Yb^{3+} in $BuMePyroTf_2N$: (—) 10 mM Yb^{3+}; (– · · –) 10 mM Yb^{2+}.

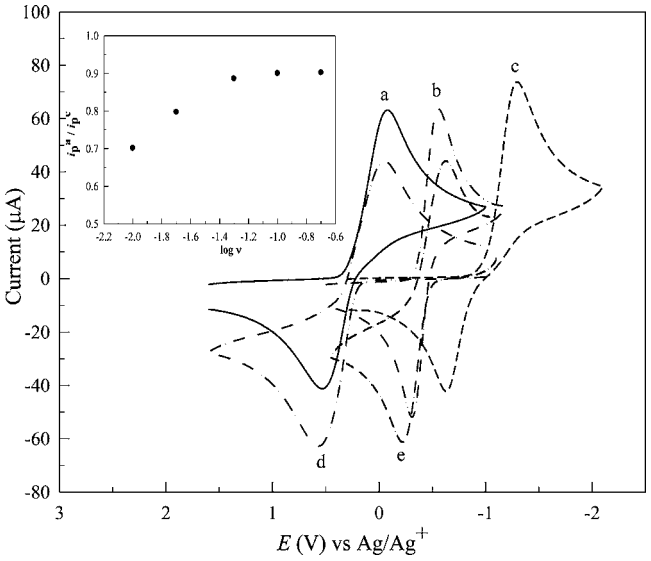

Figure 6. Cyclic staircase voltammograms of (a) 30 mM Eu^{3+}, (b) 26 mM Yb^{3+}, (c) 30 mM Sm^{3+}, (d) 30 mM Eu^{2+}, and (e) 10 mM Yb^{2+} (current × 3) in $BuMePyroTf_2N$ at 323 K. (Inset) Relationship between the peak current ratio for the reduction of Sm^{3+} and the logarithm of the scan rate.

Table 2. Voltammetric Data for $Ln^{3+/2+}$ Electrode Reactions in $BuMePyroTf_2N$ at 323 K

reaction	$E_{1/2}$ (V)[a,b]	E^0 (V)[c]	ΔE_p (V)[b]	$k^{0\prime}$ (cm s^{-1})
$Sm^{3+/2+}$	−0.964 ± 0.009	−1.55	0.51	
$Eu^{3+/2+}$	0.24 ± 0.01	−0.35	0.41	6.2×10^{-5}
			0.28[d]	8.6×10^{-6} [d]
$Yb^{3+/2+}$	−0.429 ± 0.004	−1.05	0.19	3.3×10^{-5}

[a]Potential versus Ag/Ag^+. [b]Values measured at a scan rate of 10 mV s^{-1}. [c]Potential versus SHE in aqueous solution (ref 16). [d]Measured by cyclic voltammetry (ref 30).

experimental data set to obtain spectra that were amenable to interpretation. Fitting statistics for the baseline treated in this fashion with eq 2 were quite good with the square of the

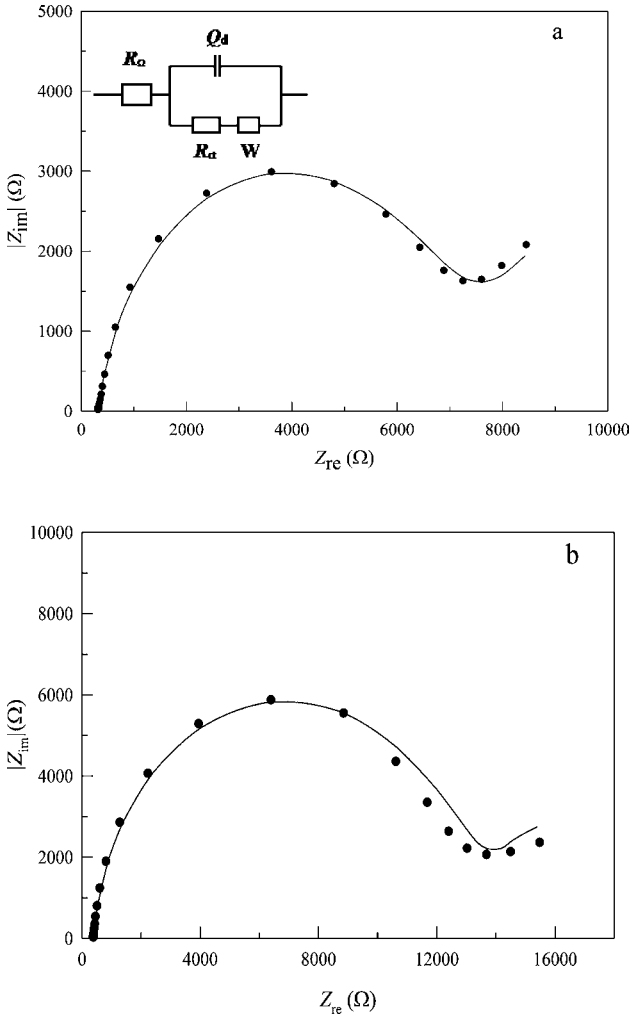

Figure 7. Complex plane impedance plots recorded at a GC electrode in $BuMePyroTf_2N$ containing (a) 10 mM Eu^{2+} + 10 mM Eu^{3+} and (b) 10 mM Yb^{2+} + 10 mM Yb^{3+}. The solid line represents the Randles-Erschler equivalent circuit model.

correlation coefficient, R^2, averaging 0.999 for all correction procedures employed herein. Figure 2b shows the spectrum in Figure 2a after application of the background correction procedure described above. This method was found to be effective for resolving very weak absorption bands > 230 nm. (The UV cutoff of the ionic liquid is about 210–220 nm.)

Trivalent europium has six electrons occupying the 4f orbital, and the ground state is $^7F_0$. Although Eu^{3+} shows several absorption bands between 360 and 600 nm, some of these bands are very weak and difficult to observe under our experimental conditions.[37] However, a weak absorption band located at 395 nm can be observed in Figure 2b, which corresponds to the process with the largest oscillator strength in the Eu^{3+} spectrum, namely, the $^5L_6 \leftarrow {}^7F_0$ transition.[22,43] The molar absorptivity at 395 nm was estimated to be about 1.8 L mol^{-1} cm^{-1}, which is comparable to the values reported for Eu^{3+} in acetonitrile (3.1 L mol^{-1} cm^{-1})[37] and perchloric acid (3.0 L mol^{-1} cm^{-1}).[44] The bands located at 464, 525, 535, and 579 nm can be assigned to the $^5D_2 \leftarrow {}^7F_0$, $^5D_1 \leftarrow {}^7F_0$, $^5D_1 \leftarrow {}^7F_1$, and $^5D_0 \leftarrow {}^7F_0$ transitions.[43,45] The $^5D_2 \leftarrow {}^7F_0$ transition as well as the $^5D_1 \leftarrow {}^7F_1$ and $^5D_0 \leftarrow {}^7F_0$ transitions are reported to show hypersensitivity to the solvation environment with stronger complexation leading to an increase in the intensity

dx.doi.org/10.1021/ic3027557 | Inorg. Chem. 2013, 52, 3241−3252

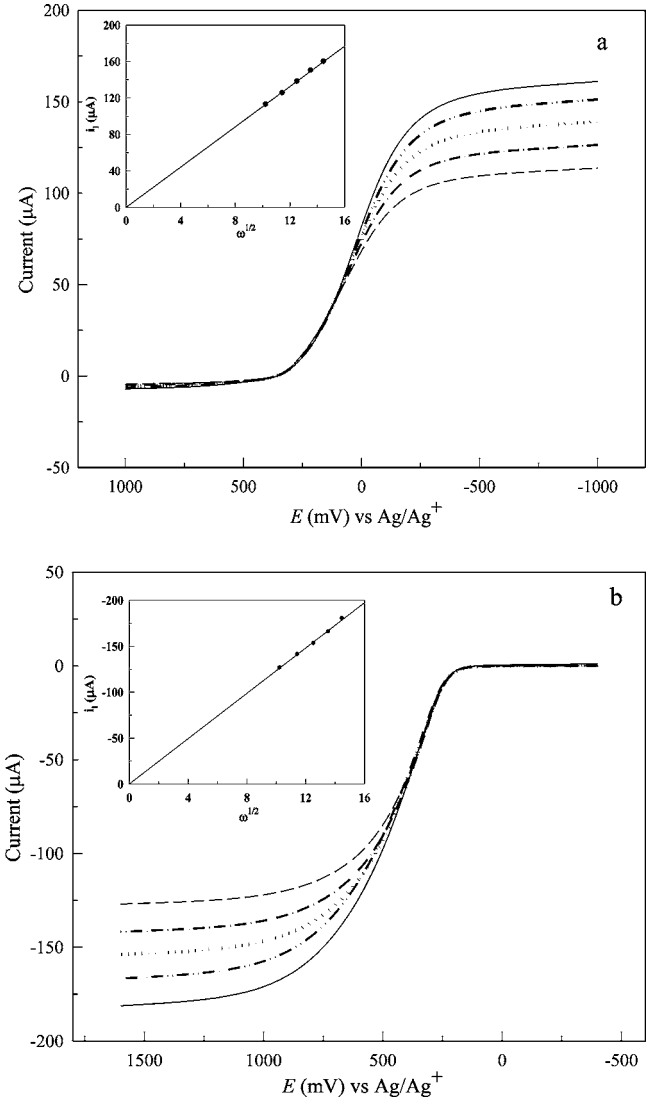

Figure 8. RDE voltammograms for (a) 30 mM Eu^{3+} and (b) 32 mM Eu^{2+} in $BuMePyroTf_2N$ at 323 K. The angular frequency of the electrode was (– –) 105, (– · –) 131, (· · ·) 157, (– · · –) 183, and (—) 209 rad s^{-1}. (Inset) Levich plots constructed from the limiting current data in each figure.

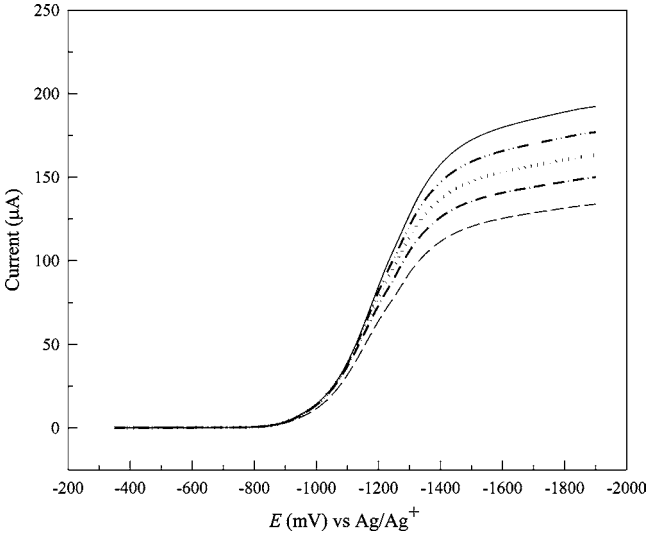

Figure 9. RDE voltammograms for 32 mM Sm^{3+} in $BuMePyroTf_2N$ at 323 K. Angular frequency of the electrode was (– –) 105, (– · –) 131, (· · ·) 157, (– · · –) 183, and (—) 209 rad s^{-1}.

of these bands.[46−48] In $BuMe_3NTf_2N$, the intensity of the $^5D_2 \leftarrow {}^7F_0$ transition at 464 nm is markedly more intense relative to the $^5L_6 \leftarrow {}^7F_0$ transition, ca. 1:8 (Figure 2b) compared to what is found in the spectrum of Eu^{3+} dissolved in aqueous $HClO_4$ where it is ∼1:50.[17] However, it is less intense than the corresponding band observed in the spectrum of Eu^{3+} dissolved in molten $LiNO_3$−KNO_3 eutectic at 423 K, where the ratio is inverted to 0.6:1.[49] The absorption bands for the two other purported hypersensitive transitions are very weak. The intensities of these bands do not seem to be significantly enhanced compared to the corresponding bands seen for Eu^{3+} in aqueous solution. Taken together, these results suggest that Eu^{3+} is probably weakly solvated in this IL, perhaps as a species such as $[Ln(Tf_2N)_x]^{(x-3)-}$.[50,51]

Spectra of a 50 mM Sm^{3+} solution in $BuMe_3NTf_2N$ before and after background correction are shown in Figure 3. The latter shows numerous absorption bands between 300 and 1100 nm. Trivalent samarium has five electrons occupying the 4f orbital, and the ground state is $^6H_{5/2}$. However, most of the 4f ← 4f bands are located between 300 and 500 nm (Figure 3b). The highest intensity band at 402 nm corresponds to the $^6P_{3/2} \leftarrow {}^6H_{5/2}$ transition.[43] The molar absorptivity of this band was estimated to be 3.8 L mol^{-1} cm^{-1}, which is very close to that found in perchloric acid (3.3 L mol^{-1} cm^{-1})[44] but smaller than that reported in acetonitrile (7.2 L mol^{-1} cm^{-1}).[37] Some of the other electronic transitions that can be reasonably assigned from the spectra in Figure 3 include $^4D_{3/2}$, $^4P_{5/2} \leftarrow {}^6H_{5/2}$ (363 nm), $^5P_{7/2}$, $^4L_{17/2}$, $^4D_{1/2} \leftarrow {}^6H_{5/2}$ (376 nm), $^4I_{13/2} \leftarrow {}^6H_{5/2}$ (462 nm), $^4I_{9/2} \leftarrow {}^6H_{5/2}$ (478 nm), $^6F_{11/2} \leftarrow {}^6H_{5/2}$ (945 nm), $^6F_{9/2} \leftarrow {}^6H_{5/2}$ (1085 nm). Sm^{3+} is also known to exhibit a hypersensitive $^4F_{1/2}$, $^4F_{3/2} \leftarrow {}^6H_{5/2}$ transition at 1563 nm.[46] Unfortunately, this band is outside the range of our spectrometer. The sensitivity of the other 4f ← 4f transitions listed above to solvation is not clear. Thus, any inferences about the solvation of Sm^{3+} in $BuMe_3NTf_2N$ must be based on the close similarities of the spectra in Figure 3b to those recorded in conventional solvents and the results for Eu^{3+}.

Figure 4 shows electronic absorption spectra of a 30 mM solution of Yb^{3+} in $BuMePyroTf_2N$ before and after background correction. In this case, the background correction method gave good results only at higher wavelengths (>∼600 nm). This spectrum shows only a weak band at 976 nm (4.4 L mol^{-1} cm^{-1}) and a shoulder at 942 nm; the bands appearing at lower wavelengths seem to be artifacts associated with the background correction procedure. For Yb^{3+} dissolved in aqueous $HClO_4$, a band is found at 974 nm (2.1 L mol^{-1} cm^{-1}) with a shoulder at ∼940 nm.[44] Yb^{3+} has 13 electrons occupying the 4f orbitals; the energy levels of the 4f configuration of this ion are the same as those for Ce^{3+}, which has only one electron in the f orbital. The Yb^{3+} ground state is $^2F_{7/2}$; the band at 976 nm in Figure 4b can therefore be assigned to the $^2F_{5/2} \leftarrow {}^2F_{7/2}$ transition.[43] Given the similarity of the spectrum recorded in the IL to that reported for Yb^{3+} in aqueous, noncomplexing media, it is very likely that Yb^{3+}, like Eu^{3+} and Sm^{3+}, is only weakly solvated by Tf_2N^- in the ILs. However, an alternate explanation is that the 4f ← 4f transition listed above is not very sensitive to the solvation environment.

The absorption spectra given in Figure 5 show the changes associated with the reduction of Yb^{3+} to Yb^{2+} by CPE at E_{app} =

dx.doi.org/10.1021/ic3027557 | Inorg. Chem. 2013, 52, 3241−3252

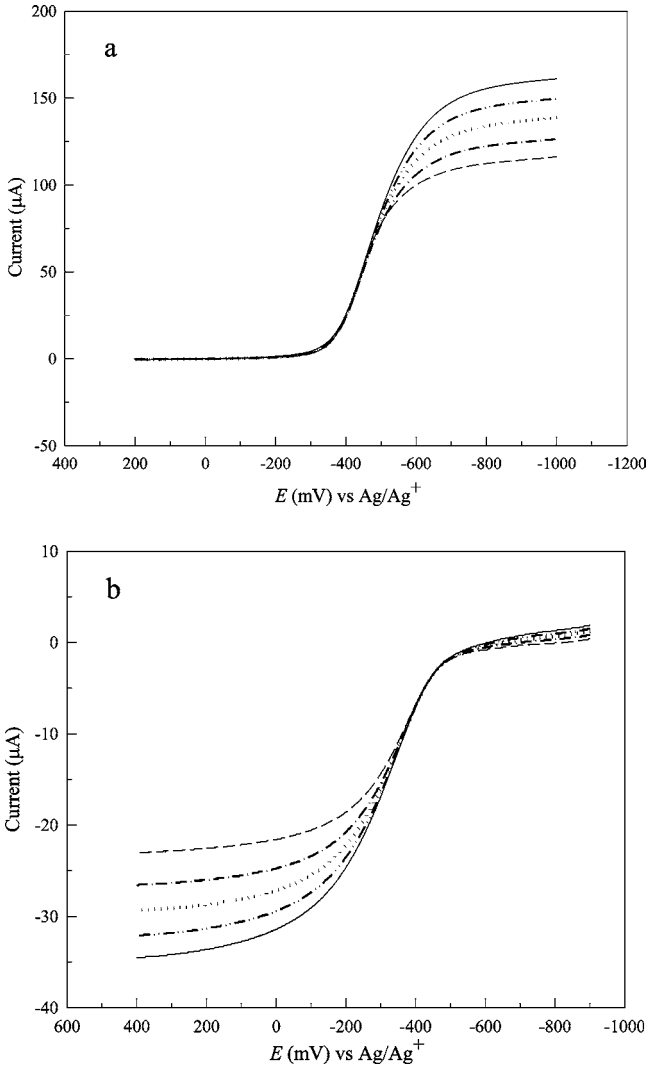

Figure 10. RDE voltammograms for (a) 30 mM Yb^{3+} and (b) 6.5 mM Yb^{2+} in $BuMePyroTf_2N$ at 323 K. Angular frequency of the electrode was (– –) 105, (– · –) 131, (· · ·) 157, (– · · –) 183, and (—) 209 rad s^{-1}.

Table 3. Diffusion Coefficient Data for Lanthanide Ions

	$10^{10}D\eta/T$ (g cm s^{-2} K^{-1})					
T(K)	Sm^{3+}	Eu^{2+}	Eu^{3+}	Yb^{2+}	Yb^{3+}	ref
323	1.06[a]	1.07[a]	1.08[a]	1.04[a]	1.10[a]	this work
303	1.04[b]	1.03[b]	1.06[b]		1.09[b]	this work
298	1.4[c]		1.3[c]		1.2[c]	28
298	1.2[d]		1.2[d]		1.1[d]	28
298			1.4[e]			28
298			1.2[f]			28
313		1.7[g]	2.3[g]			52
300				1.1[g]	1.7[g]	53
313	1.26[h]			1.26[h]	1.44[h]	54
313	1.44[i]			1.75[i]	1.39[i]	54

[a] $BuMePyroTf_2N$, RDE. [b] $BuMe_3NTf_2N$, RDE. [c] $BuMePyroTf_2N$, CA. [d] $BuMePyroTf_2N$, CP. [e] $EtMeImTf_2N$, CA. [f] $EtMeImTf_2N$, CP. [g] $AlCl_3$–EtMeImCl (N = 0.667), RDE. [h] $AlCl_3$–BuPyCl (N = 0.65), CV. [i] $AlCl_3$–BuPyCl (N = 0.65), CA.

−1.2 V. As expected, at the 10 mM concentration employed during these experiments, no absorption bands are discernible

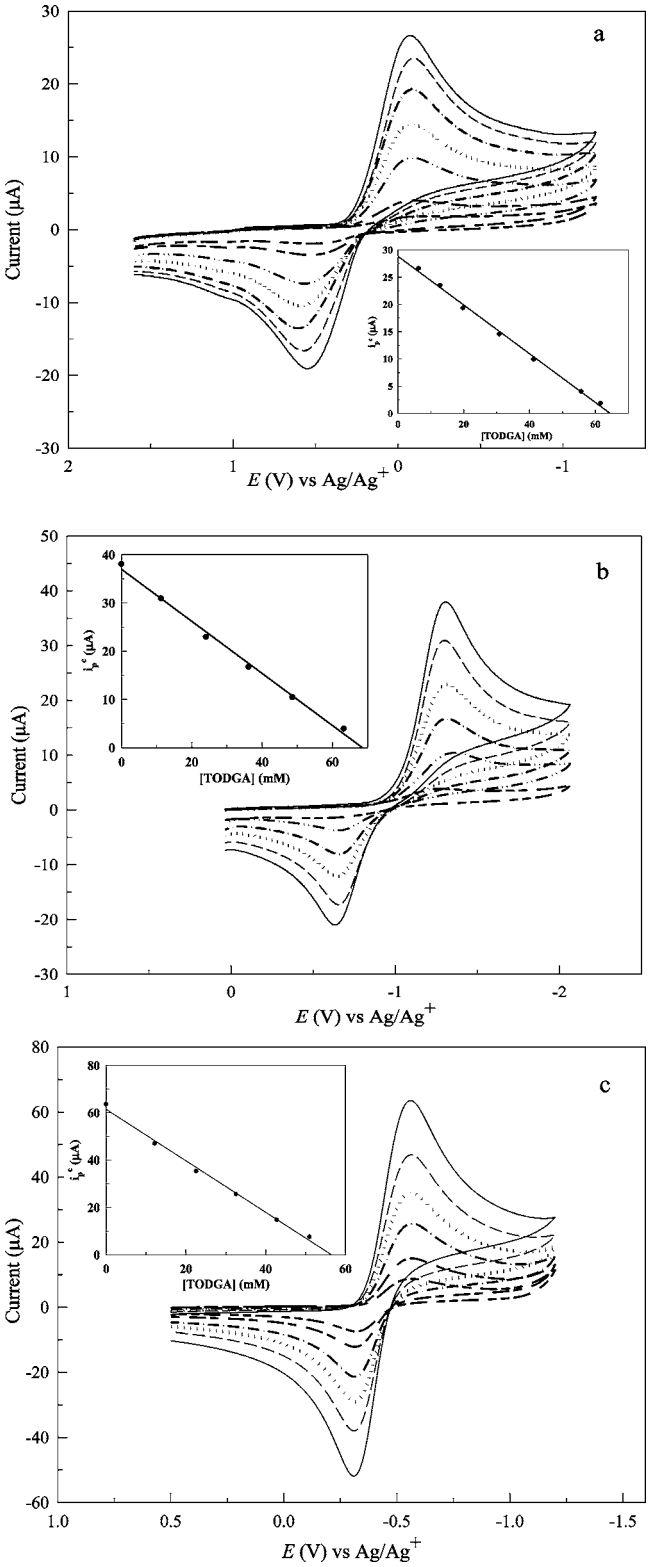

Figure 11. Cyclic staircase voltammograms of (a) 20 mM Eu^{3+}, (b) 22.6 mM Sm^{3+}, and (c) 26 mM Yb^{3+} in $BuMePyroTf_2N$ as a function of the TODGA concentration. (Insets) Plots of the Ln^{3+} reduction peak current versus the TODGA concentration.

for Yb^{3+}. However, after Yb^{3+} has been completely reduced to Yb^{2+}, two moderately intense absorption bands are apparent at around 250 (640 L mol^{-1} cm^{-1}) and 345 nm (490 L mol^{-1} cm^{-1}) as well as a weaker band at 281 nm with a shoulder at

dx.doi.org/10.1021/ic3027557 | Inorg. Chem. 2013, 52, 3241−3252

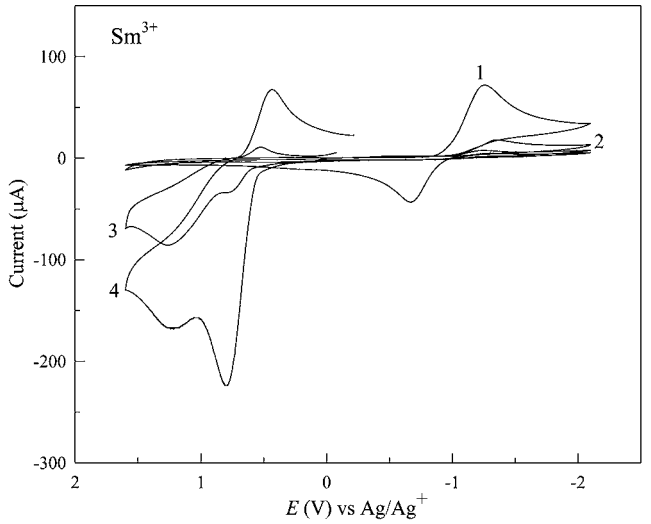

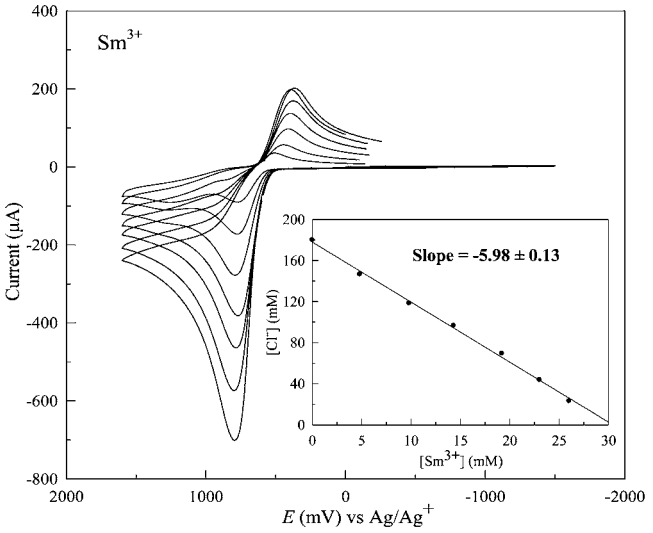

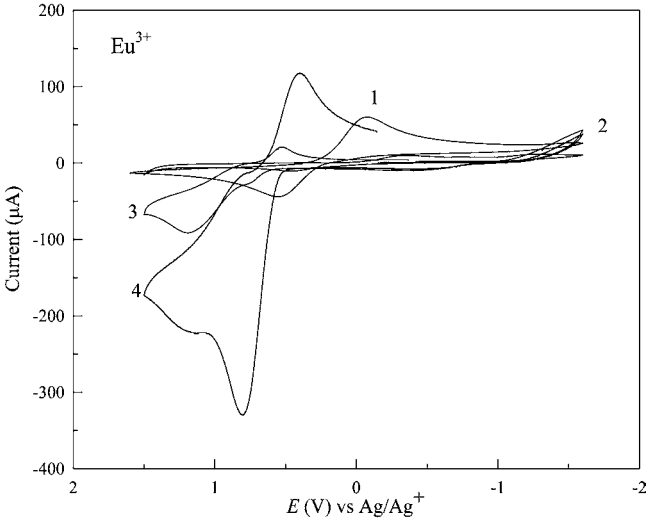

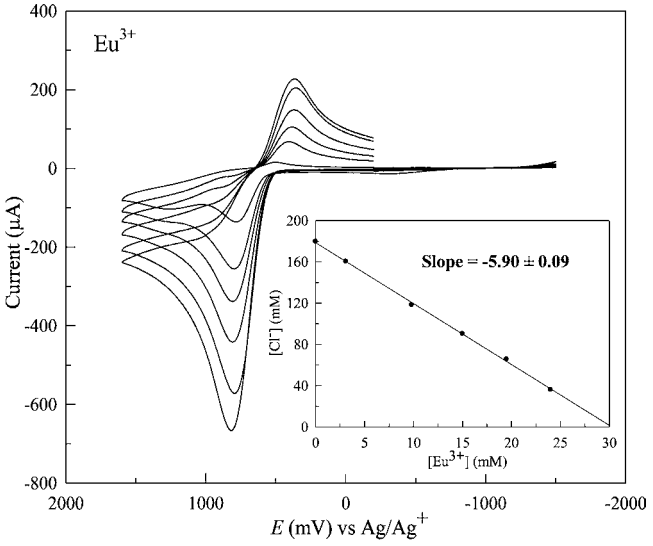

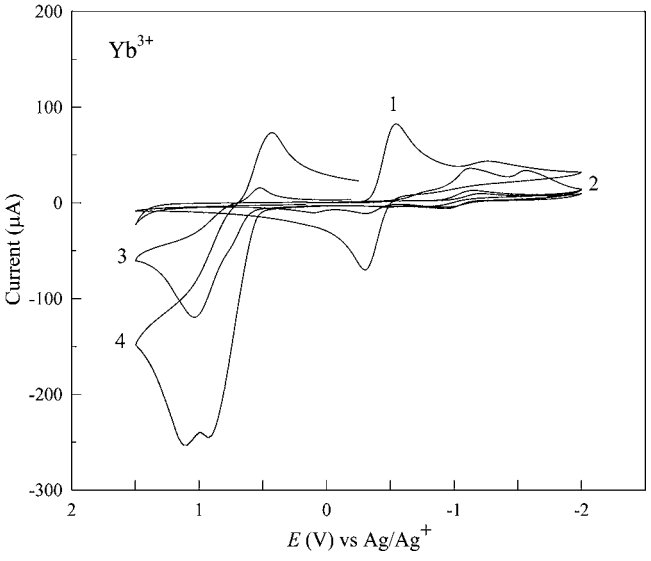

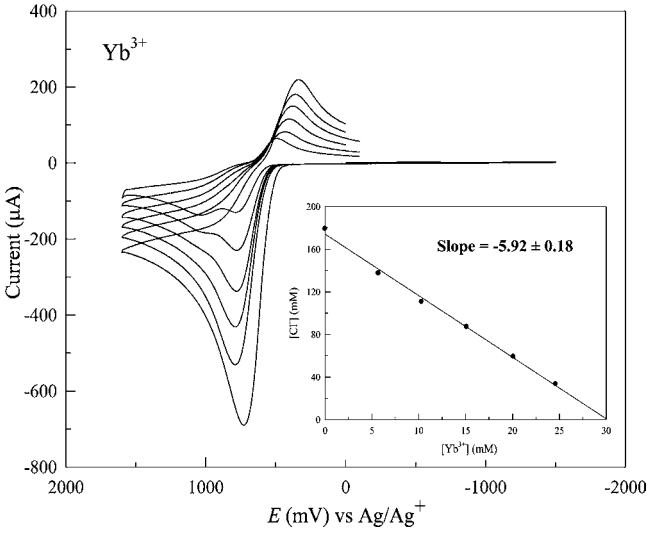

Figure 12. Cyclic staircase voltammograms at a Pt electrode in $BuMePyroTf_2N$ containing (1) 30 mM Ln^{3+}, (2) 30 mM Ln^{3+} + 90 mM Cl^- (mCl^-/mLn^{3+} = 3), (3) 30 mM Ln^{3+} + 180 mM Cl^- (mCl^-/mLn^{3+} = 6), and (4) 30 mM Ln^{3+} + 240 mM Cl^- (mCl^-/mLn^{3+} = 8). Scan rate was 50 mV s^{-1}.

Figure 13. Cyclic staircase voltammograms as a function of the Ln^{3+} concentration recorded at a Pt electrode in $BuMePyroTf_2N$ containing 180 mM BuMePyroCl. (Insets) Plots of the Cl^- concentration versus the Ln^{3+} concentration. Scan rate was 50 mV s^{-1}.

dx.doi.org/10.1021/ic3027557 | Inorg. Chem. 2013, 52, 3241−3252

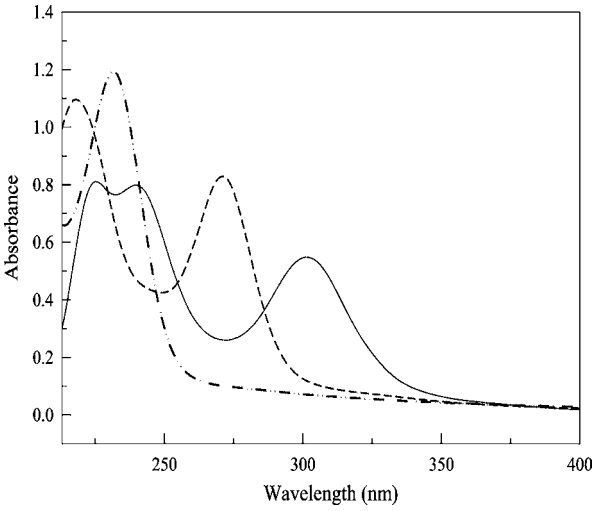

Figure 14. Electronic absorption spectra of Ln^{3+} ions recorded in $BuMePyroTf_2N$ + BuMePyroCl with $mCl^-/mLn^{3+} \geq 6$: (—) Eu^{3+}, (– · · –) Sm^{3+}, and (– –) Yb^{3+}.

~310 nm. The former bands compare favorably to those reported at 246 and 352 nm for $YbCl_2$ dissolved in H_2O.[39] These bands are most likely due to $4f^{13}5d \leftarrow 4f^{14}$ transitions, where the excited configuration is split by the ligand field of Tf_2N^- into several levels given by $J_1\Gamma_n$.[38,52] Thus, the spectrum of Yb^{2+} in $BuMePyroTf_2N$ is very similar to the spectra reported for Yb^{2+} in aqueous solutions.[39,44,53]

Voltammetry of Lanthanide Ions. Cyclic staircase voltammograms of solutions of Sm^{3+}, Eu^{2+}, and Yb^{3+} ions in the neat IL are shown in Figure 6. These solutions were prepared by the CPE coulometric oxidation of the respective metal electrodes as described above. Also shown in Figure 6 are voltammograms for a solution of Eu^{3+} that was prepared by CPE oxidation of Eu^{2+} as well as a solution of Yb^{2+} that was prepared by the reduction of Yb^{3+}. In all cases, the voltammetric peak currents for reduction/oxidation of these lanthanide ions varied linearly with concentration at a fixed CSV scan rate. The voltammetric half-wave potentials, $E_{1/2} = (E_{pa} + E_{pc})/2$, and peak potential differences, $\Delta E_p = E_{pa} - E_{pc}$, where E_{pa} and E_{pc} are the anodic and cathodic peak potentials, respectively, for the $Sm^{3+/2+}$, $Eu^{3+/2+}$, and $Yb^{3+/2+}$ redox couple are given in Table 2. Overall, these voltammetric results are quite similar to those reported previously[27,28,30] in that all three of these couples exhibit values of ΔE_p considerably larger than expected for a one-electron Nernstian electrode process at 323 K, which is ~0.064 V. Thus, all three reactions are quasireversible at best. An EIS investigation of the heterogeneous electron-transfer kinetics of the $Eu^{3+/2+}$ and $Yb^{3+/2+}$ redox reactions is presented below. It is also notable that the distribution of $E_{1/2}$ for the $Sm^{3+/2+}$, $Eu^{3+/2+}$, and $Yb^{3+/2+}$ redox couples, i.e., differences in the potential values of these couples in the IL, closely follows the differences in E^0 in aqueous solutions (Table 2).

With consideration of the spectroscopic results presented above, the CSVs in Figure 6 suggest that the $Eu^{3+/2+}$ and $Yb^{3+/2+}$ redox reactions correspond to the following general process

$$[Ln(Tf_2N)_x]^{(x-3)-} + e^- \rightleftharpoons [Ln(Tf_2N)_y]^{(y-2)-} + (x-y)Tf_2N^- \quad (3)$$

with $x \geq y$. Although solutions of Sm^{2+} cannot be prepared by CPE reduction of Sm^{3+}, the corresponding voltammogram in Figure 6 indicates that the former exhibits at least modest stability on the voltammetric time scale, especially at faster scan rates. For example, the plot of the anodic to cathodic peak current ratio, i_{pa}/i_{pc}, for the $Sm^{3+/2+}$ reaction shown in the inset of Figure 6 is ~1 at 200 mV s^{-1} but decreases as the scan rate is decreased. Thus, in a short time window, the $Sm^{3+/2+}$ reaction may follow the pathway indicated in eq 3, but over a longer period of time, Sm^{2+} most likely disproportionates to Sm^{3+} and Sm^0. This would explain why it is not possible to prepare stable solutions of Sm^{2+} in this IL. The observation that it is not possible to produce a stable deposit of Sm^0,[27] which was also verified during the present investigation, indicates that any metallic samarium produced during this disproportionation reaction most likely reacts with the IL, i.e., Sm^0 is not thermodynamically stable in the IL used for this study as discussed above.

Heterogeneous Kinetics of the $Eu^{3+/2+}$ and $Yb^{3+/2+}$ Redox Reactions. As noted above, the $Sm^{3+/2+}$, $Eu^{3+/2+}$, and $Yb^{3+/2+}$ reactions are clearly quasireversible. One problem with measuring the heterogeneous electron-transfer kinetics of redox reactions with transient techniques such as CSV in ILs such as $BuMe_3NTf_2N$ and $BuMePyroTf_2N$ is the large resistance resulting from the relatively low conductivity of these solvents.[34] This problem leads to large values of the uncompensated solution resistance, R_Ω, which are difficult to mitigate with the positive feedback compensation feature included with most potentiostats. However, EIS, which can probe redox reactions as a function of angular frequency, ω, provides a convenient method for separating R_Ω from the charge transfer resistance, R_{ct}. As shown by the equation given below, R_{ct} leads directly to the formal heterogeneous electron–transfer rate constant, $k^{0\prime}$, where C_O^* and C_R^* represent the bulk concentrations of the oxidized (Ln^{3+}) and reduced (Ln^{2+}) species, respectively

$$k^{0\prime} = RT/(nF^2AC_O^{*(1-\alpha)}C_R^{*\alpha}R_{ct}) \quad (4)$$

When $C_O^* = C_R^* = C_t^*$, the redox system is poised at its equilibrium formal potential, $E^{0\prime}$, and this equation simplifies to

$$k^{0\prime} = RT/(nF^2AC_t^*R_{ct}) \quad (5)$$

Thus, this technique is ideally suited to the investigation of $Eu^{3+/2+}$ and $Yb^{3+/2+}$. Figure 7 shows complex plane impedance plots recorded at a GC disk electrode in two solutions, one containing equimolar concentrations of Eu^{3+} and Eu^{2+} and the other equimolar concentrations of Yb^{3+} and Yb^{2+}. In both cases, data were analyzed with the Randles–Erschler equivalent circuit model[54] (Figure 7, inset), except that in the case of the interfacial capacitance better results were obtained by substituting a constant phase element Q_d[54] for the pure capacitance that is normally used in this model. The resulting values of R_{ct}, R_Ω, and Q_d were used to generate the solid lines in Figure 7. These lines show that this model provides a reasonably good representation of the experimental data. The estimates of $k^{0\prime}$ that were calculated from R_{ct} and C_t^* using eq 5 are given in Table 2. Because the electrochemistry of lanthanides in the IL solvents used in this study is a developing research area, there is not much data about the kinetics of lanthanide electrode reactions for comparison purposes. However, an estimate of $k^{0\prime}$ for the $Eu^{3+/2+}$ reaction that was measured with cyclic voltammetry based on measurements of

dx.doi.org/10.1021/ic3027557 | Inorg. Chem. 2013, 52, 3241–3252

ΔE_p was about 1 order of magnitude smaller than that found during this investigation with EIS (Table 2).[30] The smaller value of $k^{0\prime}$ may be an artifact arising from the contribution of uncompensated solution resistance to the observed value of ΔE_p.

Mass Transport of Lanthanide Ions. Rotating disk electrode voltammetric waves as a function of rotation rate for two solutions separately containing 30 mM Eu^{3+} and 32 mM Eu^{2+} in BuMePyroTf_2N are shown in Figure 8. The limiting currents, i_l, for the reduction of Eu^{3+} and the oxidation of Eu^{2+} scaled linearly with the square root of the electrode rotation rate according to the Levich equation

$$|i_l| = 0.620nFAD^{2/3}\omega^{1/2}\nu^{-1/6}C^* \quad (6)$$

where A is the electrode area (cm^2), ω is the angular frequency of the electrode (rad s^{-1}), ν is the kinematic viscosity (cm^2 s^{-1}) of the IL, and C^* represents the bulk concentration (mol cm^{-3}) of the lanthanide ions of interest. Plots of i_l versus $\omega^{1/2}$ based on the limiting currents in Figure 8 are shown in the inset of this figure. These results indicate that these redox systems are under convective mass transport control in the potential region where the limiting current is observed. Diffusion coefficients of Eu^{3+} and Eu^{2+} were calculated from the slopes of these plots and found to be very close in value, 1.19×10^{-7} and 1.16×10^{-7} cm^2 s^{-1}, respectively. Similar RDEV experiments were carried out with Sm^{3+}, Yb^{3+}, and Yb^{2+}, and the resulting voltammograms are shown in Figures 9 and 10. Plots of $|i_l|$ versus $\omega^{1/2}$ based on the limiting currents in Figures 9 and 10 were also linear and similar in appearance to those shown in Figure 8. Diffusion coefficients for Sm^{3+}, Yb^{3+}, and Yb^{2+} were calculated with the same procedure used for Eu^{2+} and Eu^{3+} and found to be 1.15×10^{-7}, 1.24×10^{-7}, and 1.14×10^{-7} cm^2 s^{-1}, respectively, at 323 K.

The classic Stokes–Einstein equation for the "perfect stick" model, in which the radius of the diffusing species is larger than the solvent molecules, is given below

$$D\eta/T = k/6\pi r_s \quad (7)$$

In this expression, η is the absolute viscosity, k is the Boltzmann constant, and r_s is the Stokes or hydrodynamic radius of the diffusing species. This relationship has been applied to the diffusion of ions in ionic liquids with good results.[32] Most importantly, estimates of $D\eta/T$ provide a convenient parameter for comparing D for a given species with results collected at different temperatures and/or in media with different viscosities provided that r_s remains constant. Values of $D\eta/T$ derived from the present investigation are summarized in Table 3 along with data derived from several literature articles.[28,55,56] (Also shown in the table are data for measurements conducted in the Lewis-acidic $AlCl_3$–EtMeImCl ionic liquid.) When $D\eta/T$ was not given directly in the cited literature article, we used the published value of D and the best estimates of η that were available at the temperature of the measurements for the IL in question. All considered, mass transport data recorded in Tf_2N-based ILs are in remarkably good agreement, with the average value of $D\eta/T$ for all data being $1.2 \pm 0.1 \times 10^{-10}$ g cm s^{-2} K^{-1} at the 95% confidence level. Thus, on the basis of eq 7, the Stokes radii of the diffusing lanthanide ions is ~610 pm. This r_s is comparable to that found for the relatively large $Ru(bpy)_3^{2+}$ ion (590 pm) in this same ionic liquid.[32] The ionic radii of the divalent and trivalent lanthanide cations examined in this investigation range from 87 pm for Yb^{3+} to 117 pm for Eu^{2+}, whereas the effective radius of Tf_2N^-, as a sphere, was estimated from molecular mechanics calculations to be ~340 pm.[57] Thus, the r_s value resulting from this investigation clearly shows that the lanthanide cations diffuse in association with Tf_2N^- anions.

Coordination of Lanthanide Ions by TODGA. The coordination of trivalent lanthanide ions by the neutral ligand TODGA was probed by conducting amperometric titration experiments. In these experiments, the solution concentrations of the ions of interest were monitored with CSV as known amounts of TODGA were added to each solution. This technique is similar to that recently employed to investigate the complexation of Ce^{3+} by Cl^-.[25] It is based on the linear relationship between the CSV reduction peak current for the reaction in eq 3 and the Ln^{3+} solution concentration. Figure 11 shows voltammograms of solutions containing fixed amounts of Eu^{3+}, Sm^{3+}, and Yb^{3+} that were recorded at the same scan rate after addition of various amounts of TODGA. When TODGA was added to each solution, the reduction currents of the $[Ln(Tf_2N)_x]^{(x-3)-}$ species decreased commensurately. No waves for the resulting complexed ions could be observed within the potential window of the solvent. Thus, the positive change in ΔG associated with formation of lanthanide–TODGA complexes shifts the lanthanide ion reduction process to substantially more negative potentials, indicating that the stability constant for such complexes must be quite large in the IL. In addition, as the amount of TODGA added to each of the Ln^{3+} solutions was increased to the concentration necessary to complex about 50% of the Ln^{3+}, phase separation was observed with the resulting Ln^{3+}–TODGA complex forming a second, less dense layer in the electrochemical cell.

The inset of each series of CSV waves in Figure 11 shows a plot of the reduction peak currents for these ions versus the TODGA concentration. The slopes of these plots give a direct measure of the stoichiometry of the complexes formed between the Ln^{3+} ions and TODGA. They indicate that TODGA forms 3:1 complexes with Sm^{3+} and Eu^{3+}; however, the smaller Yb^{3+} ion forms a 2:1 complex. This result is somewhat different from that found during liquid–liquid extraction experiments from aqueous HNO_3 with La^{3+}, Eu^{3+}, and Lu^{3+} in EtMeImTf_2N.[9] In this case, all three ions, including the heavier but smaller Lu^{3+} ion, were found to form 3:1 complexes with TODGA. By comparison, experiments involving extraction of Sm^{3+}, Eu^{3+}, and Yb^{3+} from aqueous HNO_3 with TODGA in *n*-dodecane indicated formation of 4:1 complexes. Interestingly, we found that Eu^{2+} is also complexed by TODGA in the IL, but the electrochemical signature of the resulting complex is visible in the IL potential window and not shifted strongly to more negative potentials. This indicates that the resulting Eu^{2+}–TODGA complex is considerably less stable than the corresponding Eu^{3+}–TODGA complex. At this point it is not clear whether the contrasting stoichiometry revealed during these electrochemical investigations reflects the methods used for the measurements or represents actual differences in the chemistry, e.g., differences associated with the presence of aqueous ions or acidic species such as HNO_3 in extraction experiments.

Coordination of Lanthanide Ions by Cl^-. The coordination of Sm^{3+}, Eu^{3+}, and Yb^{3+} by Cl^- in the ILs was probed by carrying out amperometric titration experiments like those conducted with TODGA. However, in these experiments, weighed portions of a Cl^- source, BuMePyroCl, were added to individual solutions of these Ln^{3+} ions while observing the voltammetric signatures of the resulting solutions with CSV.

dx.doi.org/10.1021/ic3027557 | Inorg. Chem. 2013, 52, 3241–3252

Examples of the voltammograms resulting from these experiments are given in Figure 12. Each of the Ln^{3+} solutions gave similar results. Furthermore, these results were comparable to those found in BuMePyroTf$_2$N solutions containing Ce^{3+}, Pr^{3+}, and Nd^{3+} following addition of BuMePyroCl.[25,35] For example, when the mole ratio of Cl^- to Ln^{3+}, mCl^-/mLn^{3+}, reaches ~3, the CSV reduction peak currents for each of the Ln^{3+} ions greatly diminishes and the solutions become cloudy due to formation of finely divided white precipitates. Although we did not collect and analyze these precipitates, we infer from previous work with Ce^{3+} that this solid material corresponds to the insoluble trivalent chloride compounds, $LnCl_3$.[25] When mCl^-/mLn^{3+} is increased to about 4.5 by addition of more BuMePyroCl, most of the precipitate redissolves, the original reduction waves for the $Ln^{3+/2+}$ reactions in the neat IL disappear, and new, poorly defined oxidation waves appear at very positive potentials. Finally, when $mCl^-/mLn^{3+} > 6$, a new wave corresponding to the quasireversible oxidation of Cl^- that is not coordinately bound to Ln^{3+} can be seen in each solution at $E_p^a = 0.75$ V.

In order to further explore the coordination of trivalent lanthanides in solutions containing excess Cl^-, we carried out amperometric titration experiments in which Ln^{3+} was added coulometrically to BuMePyroTf$_2$N solutions containing large, fixed amounts of BuMePyroCl. Figure 13 shows the voltammograms recorded during these experiments. As demonstrated previously, the Cl^- oxidation current in these ionic liquids varies linearly with the Cl^- concentration over the concentration range typically employed during these experiments.[25] A plot of the chloride concentration versus the Ln^{3+} concentration resulting from these experiments is given in the inset of each series of voltammograms shown in Figure 13. In each case, the slopes of these plots are ~6, indicating that Cl^- coordinates with the trivalent lanthanides in this IL to form $[LnCl_6]^{3-}$ ions.

We also examined the electronic absorption spectra of Ln^{3+} in BuMePyroTf$_2$N with $mCl^-/mLn^{3+} \geq 6$. Spectra for Sm^{3+}, Eu^{3+}, and Yb^{3+} are shown in Figure 14. The spectrum of Sm^{3+} exhibits a single absorption band (231 nm; 800 L mol^{-1} cm^{-1}), which is in close agreement with the spectrum reported for the octahedral chloride complex, $[SmCl_6]^{3-}$, in CH_3CN saturated with Et_4NCl (232 nm, 930 L mol^{-1} cm^{-1}).[58] Similarly, Eu^{3+} exhibits three moderately intense bands (301 nm, 364 L mol^{-1} cm^{-1}; 238 nm, 532 L mol^{-1} cm^{-1}; 226 nm, 540 L mol^{-1} cm^{-1}), two of which compare favorably with the classical spectrum of $[EuCl_6]^{3-}$ in CH_3CN saturated with Et_4NCl (301 nm, 400 L mol^{-1} cm^{-1}; 235 nm, 640 L mol^{-1} cm^{-1}).[58] (Note: the band we found at 226 nm is not reported in the literature and probably appears below the UV cutoff of CH_3CN saturated with Et_4NCl.) Finally, Yb^{3+} exhibits two bands (271 nm, 166 L mol^{-1} cm^{-1}; ~215 nm). The first band is in good agreement with that reported for $[YbCl_6]^{3-}$ in CH_3CN saturated with Et_4NCl (273 nm, 160 L mol^{-1} cm^{-1})[58] and in chloride-rich $AlCl_3$–EtMeImCl (268 nm, 303 L mol^{-1} cm^{-1}).[56] As is the case for the literature spectrum of $[EuCl_6]^{3-}$, the band we found at higher energy in the spectrum of Yb^{3+} is not reported in the literature, probably because it appears below the UV cutoff of the molecular solvent. Thus, these results, when taken together with the titration experiments, clearly indicate that the octahedral $[LnCl_6]^{3-}$ complexes are the limiting species in chloride-rich BuMePyroCl.

Although largely obscured by the large Cl^- oxidation wave in each of the voltammograms in Figure 12, the small poorly defined oxidation waves that are apparent at potentials more positive than the Cl^- oxidation waves when $mCl^-/mLn^{3+} \geq 6$, e.g., the waves at 1.25 (Sm^{3+}), 1.20 (Eu^{3+}), and 1.04 V (Yb^{3+}), scale linearly with the respective lanthanide ion concentration. Unfortunately, none of these waves exhibits a reverse current. A reasonable assumption is that these waves arise from oxidation of the respective $[LnCl_6]^{3-}$ complex. However, in agreement with the observed chemistry of these particular lanthanides, the products of these reactions, which might be expected to be tetravalent species such as $[LnCl_6]^{2-}$, exhibit virtually no stability on the CSV time scale. In addition, the $[LnCl_6]^{3-/4-}$ reduction reaction is not evident before the negative limit of the ionic liquid. Thus, like the stability afforded to Ln^{3+} through coordination with TODGA, coordination by chloride significantly stabilizes the Ln^{3+} species, shifting its reduction potential to more negative values.

AUTHOR INFORMATION

Corresponding Author

*E-mail: chclh@chem1.olemiss.edu

Notes

The authors declare no competing financial interest.

ACKNOWLEDGMENTS

This research was funded by the Division of Chemical Sciences, Geosciences, and Biosciences, Office of Basic Energy Science of the U.S. Department of Energy through Grant DE-AC02-98CH10886, Subcontract 154868, from Brookhaven National Laboratory.

REFERENCES

(1) Endres, F. *Electrodeposition from Ionic Liquids*; Wiley-VCH: Weinheim, 2008.

(2) Ohno, H. *Electrochemical Aspects of Ionic Liquids*; John Wiley & Sons: Hoboken, NJ, 2005.

(3) Galinski, M.; Lewandowski, A.; Stepniak, I. *Electrochim. Acta* **2006**, *51*, 5567–5580.

(4) Tsuda, T.; Hussey, C. L. In *Modern Aspects of Electrochemistry*; White, R. E., Ed.; Springer Science: New York, 2009; Vol. *45*, pp 63–174.

(5) Ha, S. H.; Menchavez, R. N.; Koo, Y.-M. *Korean J. Chem. Eng.* **2010**, *27*, 1360–1365.

(6) Venkatesan, K. A.; Rao, C. J.; Nagarajan, K.; Rao, P. R. V. *Int. J. Electrochem.* **2012**, *2012*, 1–12.

(7) Binnemans, K. *Chem. Rev.* **2007**, *107*, 2592–2614.

(8) Mudring, A.-V.; Tang, S. *Eur. J. Inorg. Chem.* **2010**, 2569–2581.

(9) Shimojo, K.; Kurahashi, K.; Naganawa, H. *Dalton Trans.* **2008**, 5083–5088.

(10) Shen, Y.; Tan, X.; Wang, L.; Wu, W. *Sep. Purif. Technol.* **2011**, *78*, 298–302.

(11) Ansari, S. A.; Mohapatra, P. K.; Manchanda, V. K. *Ind. Eng. Chem. Res.* **2009**, *48*, 8605–8612.

(12) Panja, S.; Mohapatra, P. K.; Tripathi, S. S.; Gandhi, P. M.; Janardan, P. *Sep. Purif. Technol.* **2012**, *96*, 289–295.

(13) Sengupta, A.; Mohapatra, P. K.; Iqbal, M.; Huskens, J.; Verboom, W. *Dalton Trans.* **2012**, *41*, 6970–6979.

(14) Bell, J. R.; Luo, H.; Dia, S. *Sep. Sci. Technol.* **2012**, *47*, 2002–2006.

(15) Greenwood, N. N.; Earnshaw, A. *Chemistry of the Elements*; Elsevier: Amsterdam, 2012; p 1341.

(16) Bard, A. J.; Parsons, R.; Jordan, J. *Standard Potentials in Aqueous Solutions*; Marcel Dekker: New York, 1985.

(17) Carnall, W. T. In *Handbook on the Physics and Chemistry of Rare Earths*; Geschneider, K. A., Eyring, L., Eds.; NorthHolland: Amsterdam, 1979; Vol. 3, pp 171–208.

(18) Bunzli, J.-C. G.; Piguet, C. *Chem. Soc. Rev.* **2005**, *34*, 1048–1077.

(19) Billard, I.; Moutiers, G.; Labet, A.; El Azzi, A.; Gaillard, C.; Mariet, C.; Lutzenkirchen, K. *Inorg. Chem.* **2003**, *42*, 1726−1733.
(20) Driesen, K.; Nockemann, P.; Binnemans, K. *Chem. Phys. Lett.* **2004**, *395*, 306−310.
(21) Arenz, S.; Babai, A.; Binnemans, K.; Driesen, K.; Giernoth, R.; Mudring, A. V.; Nockemann, P. *Chem. Phys. Lett.* **2005**, *402*, 75−79.
(22) Billard, I.; Mekki, S.; Gaillard, C.; Hesemann, P.; Moutiers, G.; Mariet, C.; Labet, A.; Bunzli, J. C. G. *Eur. J. Inorg. Chem.* **2004**, 1190−1197.
(23) Gaillard, C.; Billard, I.; Chaumont, A.; Mekki, S.; Ouadi, A.; Denecke, M. A.; Moutiers, G.; Wipff, G. *Inorg. Chem.* **2005**, *44*, 8355−8367.
(24) Stumpf, S.; Billard, I.; Panak, P. J.; Mekki, S. *Dalton Trans.* **2007**, 240−248.
(25) Chou, L.-H.; Cleland, W. E.; Hussey, C. L. *Inorg. Chem.* **2012**, *51*, 11450−11457.
(26) Bhatt, A. I.; May, I.; Volkovich, V. A.; Hetherington, M. E.; Lewin, B.; Thied, R. C.; Ertok, N. *Dalton Trans.* **2002**, 4532−4534.
(27) Bhatt, A. I.; May, I.; Volkovich, V. A.; Collison, D.; Helliwell, M.; Polovov, I. B.; Lewin, R. G. *Inorg. Chem.* **2005**, *44*, 4934−4940.
(28) Yamagata, M.; Katayama, Y.; Miura, T. *J. Electrochem. Soc.* **2006**, *153*, E5−E9.
(29) Nagaishi, R.; Arisaka, M.; Kimura, T.; Kitatsuji, Y. *J. Alloys Compd.* **2007**, *431*, 221−225.
(30) Rao, C. J.; Venkatesan, K. A.; Nagaishi, R.; Srinivasan, T. G.; Rao, P. R. V. *Electrochim. Acta* **2009**, *54*, 4718−4725.
(31) Babai, A.; Pitula, S.; Mudring, A.-V. *Eur. J. Inorg. Chem.* **2010**, 4933−4937.
(32) Pan, Y.; Boyd, L. E.; Kruplak, J. F.; Cleland, W. E.; Wilkes, J. S.; Hussey, C. L. *J. Electrochem. Soc.* **2011**, *158*, F1−F9.
(33) Xu, X. H.; Hussey, C. L. *J. Electrochem. Soc.* **1993**, *140*, 1226−1233.
(34) Pan, Y.; Cleland, W. E.; Hussey, C. L. *J. Electrochem. Soc.* **2012**, *159*, F125−F133.
(35) Chou, L.-H.; Hussey, C. L. *Manuscript in preparation*, 2013.
(36) Lewandowski, A.; Swiderska-Moeck, A. *J. Power Sources* **2009**, *194*, 601−609.
(37) Dyke, J. M.; Hush, N. S. *J. Electroanal. Chem.* **1972**, *36*, 337−347.
(38) Johnson, K. E.; Sandoe, J. N. *Mol. Phys.* **1968**, *14*, 595−598.
(39) Butement, F. D. S. *Trans. Faraday Soc.* **1948**, 617−626.
(40) Jiang, J.; Higashiyama, N.; Machida, K.; Adachi, G. *Coord. Chem. Rev.* **1998**, *170*, 1−29.
(41) Higashiyama, N.; Takemura, K.; Kimura, K.; Adachi, G. *Inorg. Chim. Acta* **1992**, *194*, 201.
(42) Sabbatini, N.; Ciano, M.; Dellonte, S.; Bonazzi, A.; Balzani, V. *Chem. Phys. Lett.* **1982**, *90*, 265−268.
(43) Binnemans, K.; Gorller-Walrand, C. *Chem. Phys. Lett.* **1995**, *235*, 163−174.
(44) Banks, C. V.; Klingman, D. W. *Anal. Chim. Acta* **1956**, *15*, 356−363.
(45) Carnall, W. T.; Fields, P. R.; Rajnak, K. *J. Chem. Phys.* **1968**, *49*, 4450−4455.
(46) Peacock, R. D. In *Structure and Bonding (Berlin)*; Dunitz, J., Ed.; Springer: New York, 1975; Vol. *22*.
(47) Bunzli, J.-C. G.; Eliseeva, S. V. In *Lanthanide Luminescence: Photophysical, Analytical, and Biological Aspects*, Hanninen, P., Harma, H., Eds.; Springer-Verlag: Berlin, Heidelberg, 2010.
(48) Yatsimirskii, K. B.; Davidenko, N. K. *Coord. Chem. Rev.* **1979**, *27*, 223−273.
(49) Carnall, W. T.; Gruen, D. M.; McBeth, R. L. *J. Phys. Chem.* **1962**, *66*, 2159−2164.
(50) Babai, A.; Mudring, A. V. *Chem. Mater.* **2005**, *17*, 6230−6238.
(51) Babai, A.; Mudring, A. V. *Dalton Trans.* **2006**, 1828−1830.
(52) Johnson, K. E.; Mackenzie, J. R.; Sandoe, J. N. *J. Chem. Soc. (A)* **1968**, 2644−2647.
(53) Butement, F. D. S.; Terry, H. *J. Chem. Soc.* **1937**, 1112.
(54) Orazem, M. E.; Tribollet, B. *Electrochemical Impedance Spectroscopy*; John Wiley & Sons, Inc.: Hoboken, NJ, 2008.
(55) Gau, W. J.; Sun, I. W. *J. Electrochem. Soc.* **1996**, *143*, 914−919.
(56) Gau, W. J.; Sun, I. W. *J. Electrochem. Soc.* **1996**, *143*, 170−174.
(57) Jin, H.; O'Hare, B.; Dong, J.; Azhantsev, S.; Baker, G. A.; Wishart, J. F.; Benesi, A. J.; Maroncelli, M. *J. Phys. Chem. B* **2008**, *112*, 81−92.
(58) Ryan, J. L.; Jorgensen, C. K. *J. Phys. Chem.* **1966**, *70*, 2845−2857.